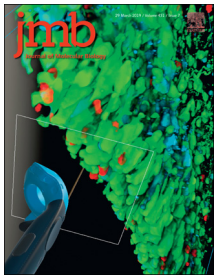

ATXR5/6 Forms Alternative Protein Complexes with PCNA and the Nucleosome Core Particle

Hossein Davarinejad [1], Monika Joshi [1], Narimane Ait-Hamou [1], Kim Munro [2] and Jean-François Couture [1]

*1 - **Ottawa Institute of Systems Biology,** Department of Biochemistry, Microbiology and Immunology, University of Ottawa, 451 Smyth Road, Ottawa, ON K1H 8M5, Canada*
*2 - **Protein Function Discovery Facility,** Queen's University, Kingston, ON K7L 3N6, Canada*

***Correspondence to Jean-François Couture:** University of Ottawa, Ottawa Institute of Systems Biology, 451 Smyth Road, Roger Guindon Hall, Ottawa, ON K1H 8M5, Canada. jean-francois.couture@uottawa.ca*
https://doi.org/10.1016/j.jmb.2019.02.020
Edited by Sepideh Khorasanizadeh

Abstract

The proliferating cell nuclear antigen (PCNA) is a sliding clamp associated with DNA polymerases and serves as a binding platform for the recruitment of regulatory proteins linked to DNA damage repair, cell cycle regulation, and epigenetic signaling. The histone H3 lysine-27 (H3K27) mono-methyltransferase *Arabidopsis* trithorax-related protein 5/6 (ATXR5/6) associates with PCNA, and this interaction has been proposed to act as a key determinant controlling the reestablishment of H3K27 mono-methylation following replication. In this study, we provide biochemical evidence showing that PCNA inhibits ATXR6 enzymatic activity. The structure of the ATXR6 PCNA-interacting peptide (PIP) in complex with PCNA indicates that a trio of hydrophobic residues contributes to the binding of the enzyme to the sliding clamp. Finally, despite the presence of three PIP binding clefts, only two molecules of ATXR6 bind to PCNA likely enabling the recruitment of a third protein to the sliding clamp. Collectively, these results rule out the model wherein PCNA-bound ATXR6 actively reestablishes H3K27 mono-methylation following DNA replication and provides insights into the role of ATXR6 PIP motif in its interaction with PCNA.

Introduction

Methylation of histone proteins is a widely observed post-translational modification linked to many nuclear transactions [1]. Among those, methylation of lysine residues plays important roles in chromatin remodeling and epigenetic signaling [2]. This post-translational modification occurs mostly on histone tails and is catalyzed by histone lysine methyltransferases, a family of enzymes typically characterized by the presence of a catalytic SET (Su[var], E[z], Trithorax) domain [3].

Methylation of K27 in histone H3 (H3K27) is predominantly associated with heterochromatin formation and found in poorly transcribed regions [4]. In mammals, H3K27 methylation is deposited by *Drosophila* E(z) homologs, EZH1/2, and regulate crucial processes such as the expression of *Hox* genes [5], which control homeotic development, X chromosome inactivation [6], and differentiation of embryonic stem cells to mesodermal stem cell lineage [7]. In plants, H3K27 methylation is catalyzed by several enzymes including MEA, CLF, SWN, and *Arabidopsis* trithorax-related proteins (ATXR) 5/6. ATXR5/6 are SET domain proteins [8] important for heterochromatin condensation [9] and regulate ribosomal RNAs [10] as well as myoinositol phosphate synthase expression [11]. In heterochromatin, ATXR5/6 also regulate DNA replication as double mutants result in over-replicated heterochromatin [12].

Mechanistically, ATXR5/6 specifically mono-methylate H3.1 [13], and post-translational modifications deposited in the vicinity of the methylation site inhibit the enzymes [14]. The PHD domain of ATXR5/6 preferentially binds the N-terminus of histone H3, and these enzymes mono-methylate H3K27 when incorporated in a nucleosome core

particle (NCP) [14]. An evolutionary conserved region connecting the SET and PHD domains in ATXR5/6 includes a consensus sequence showing high homology to the proliferating cell nuclear antigen (PCNA)-interacting peptide (PIP) motif. PCNA belongs to the DNA sliding clamp family of proteins and assembles as a homo-trimeric ring-like structure, which circles around DNA. Initially identified as a protein associating with DNA polymerase and an important regulatory factor controlling DNA replication, PCNA is now known to associate with several other proteins including epigenetic signaling and chromatin remodeling enzymes such as histone acetyltransferase (HAT) p300 [15], DNA methyltransferase 1 (DNMT1) [16], chromatin assembly factor 1 (CAF1) [17], Williams syndrome transcription factor:imitation switch/sucrose non-fermentable 2H (WSTF:ISWI/SNF2H) [18], and EZH2 [19].

Yeast two-hybrid and bi-molecular fluorescence complementation assays showed that ATXR5/6 co-localize with PCNA [20]. Studies on genomic integrity in plants also revealed that in addition to mutations in the PHD and SET domains, mutation in ATXR5/6 PIP motif disrupts chromatin organization and H3K27 methylation [12]; yet, little is known about the underlying mechanisms of ATXR5/6 PIP contribution in maintaining this important epigenetic mark. In the present study, we have determined the structure of ATXR6 PIP motif in complex with PCNA. We find that despite three occupied sites on the PCNA trimer by a peptide corresponding to ATXR6 PIP motif, only two molecules of the full-length enzyme can bind to the sliding clamp. The structure and biochemical analysis reveal how a central hydrophobic residue in the ATXR6 PIP motif confers high-affinity binding to PCNA. We also find that methylation of the NCP by ATXR6 is blocked by PCNA, suggesting that ATXR6 must dissociate from PCNA to re-establish H3K27 methylation.

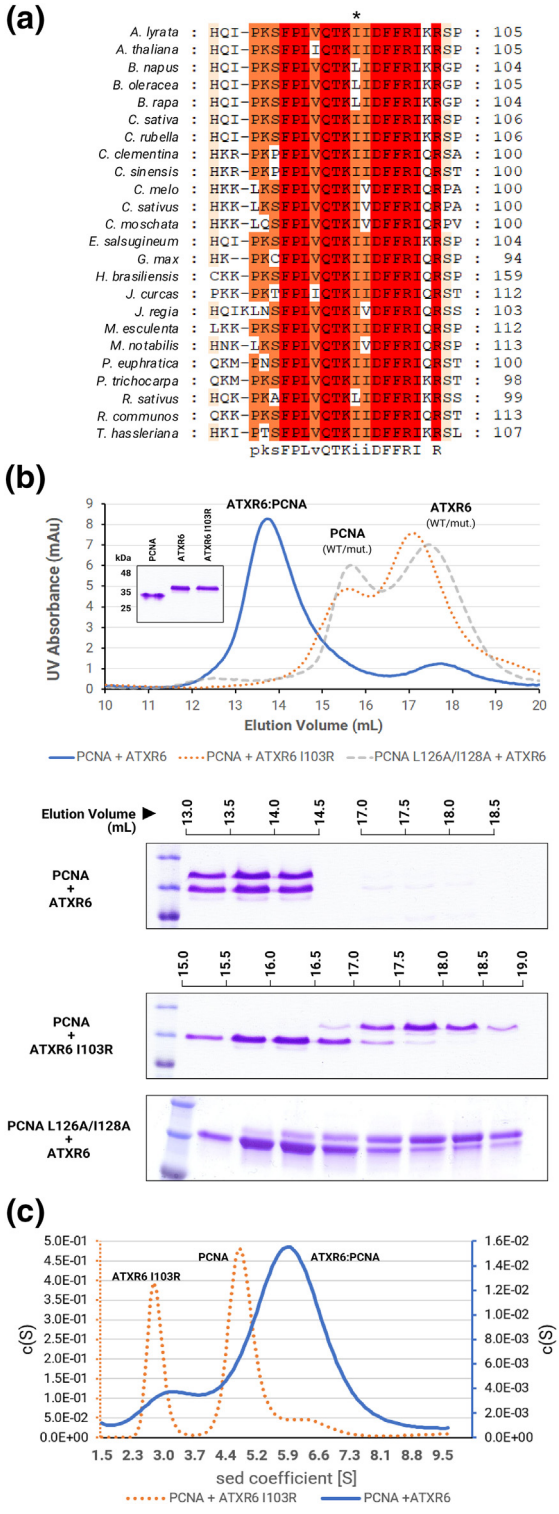

Fig. 1. ATXR6 directly associates with PCNA. (a) Sequence alignment of ATXR6 PIP motifs across multiple plant species. The asterisk indicates the isoleucine residue, or its equivalent in other ATXR6 homologs, mutated in this study. (b) Gel filtration profiles of PCNA:ATXR6 complex, PCNA + ATXR6 I103R, and PCNA L126A/I128A + ATXR6. Coomassie-stained SDS-PAGE corresponding to each peak fraction is shown below the curves. Individual proteins used in these experiments are shown as inlet overlaid on the gel filtration profiles. (c) Analytical ultracentrifugation sedimentation patterns for PCNA:ATXR6 and PCNA + ATXR6 I103R.

Results and Discussion

An evolutionary conserved motif in ATXR6 mediates its interaction with PCNA

Alignment of the region separating the PHD and SET domains of ATXR6 between 25 plant species (Fig. 1a) shows that a region comprising residues QTKIIDFF has high-sequence similarity to a peptide motif (Q-x-x-V/L/I-x-x-F/Y-F/Y) found in proteins known to interact with PCNA. To confirm that this

region directly mediates an interaction between PCNA and ATXR6, each protein was homogeneously purified, co-incubated, and separated by size exclusion chromatography. As shown in Fig. 1b, gel filtration profile shows that the protein complex elutes as a single peak with an apparent molecular weight of ~170 kDa. However, incubation of a PIP-motif mutant, *Mn*ATXR6 I103R, with PCNA yields two protein species eluting at molecular weights of ~90 and ~40 kDa. Residues Leu126/Ile128 in PCNA are critical for PIP binding but dispensable for trimerization of the protein [21]. The double mutant was purified, incubated with wild-type ATXR6, and separated by gel filtration. As demonstrated in Fig. 1b and similar to the observation made with ATXR6 PIP mutant, two peaks corresponding to the trimeric form of PCNA (L126A/I128A) and ATXR6 were observed, suggesting that both ATXR6 PIP motif and the PIP binding cleft of PCNA are important for the formation of the complex. To define the stoichiometry of the complex, ATXR6 wild-type or mutant was incubated with PCNA and separated using analytical ultracentrifugation. Incubation of wild-type ATXR6 with PCNA shows a predominant peak at an *s*-value of 6, which corresponds to an approximated molecular weight of 174 kDa. Conversely, incubation of ATXR6 I103R with PCNA shows two predominant peaks at *s*-values corresponding to 40.1 and 90.8 kDa, indicating that the mutation impairs the association of ATXR6 to PCNA. Collectively, these results suggest that ATXR6 PIP motif participates in the binding of PCNA and that two molecules of ATXR6 bind to a trimer of PCNA.

The homotrimeric nature of PCNA provides the mechanism and possibility for more than one partner to bind simultaneously. In such model previously coined as sliding clamp "tool belt" [22], a variety of PCNA partners are in the bound state and ready to engage at the site of action. Notably, studies using mutant/wild-type heterotrimers of PCNA have shown that in cases such as the Okazaki fragment maturation, inactivation of two of the three PCNA binding sites has no effect on the biological process [23], suggesting that site anchoring may not play a significant role in sequential binding of all PCNA partners. The vast majority of available stoichiometric and structural data investigating the interaction of PIP-motif proteins with trimeric PCNA are limited to analyses using a short peptide and report a 3(PIP-motif):1(PCNA trimer) ratio. Only few studies provide insight into the stoichiometry of PCNA bound to full-length proteins. For example, one molecule of RNAse HII occupies each of the three PCNA monomers in distinct orientations, but collectively, the three molecules come in close proximity to block the aperture of the DNA clamp in the absence of DNA [24]. Similarly, the crystal structure of flap endonuclease 1 (FEN-1) bound to PCNA shows the same stoichiometry of binding and captures FEN-1 in different orientations, in one of which, FEN-1 is pulled away from the PCNA central hole and supposedly inactive, and another orientation in which FEN-1 is close to the central hole where interaction with DNA is possible for endonuclease activity. Similar to ATXR6, growth arrest and DNA-damage-inducible protein 45 (Gadd45), a DNA damage response protein, binds PCNA in a 2:1 ratio [25]; however, Gadd45 does not contain a PIP-motif and no structural data are available for the full-length protein in complex with PCNA. Interestingly, unlike RNSase HII and FEN-1, ATXR6 and Gadd45 have no known activity on DNA; rather, they serve as signaling proteins. PCNA was reported to regulate the turnover of SET8 by serving as a co-recruitment hub for both SET8 and its associated E3 ligase, $CRL4^{Cdt2}$, which targets SET8 for ubiquitin-mediated proteasomal degradation [26,27]. Akin to SET8, ATXR5/6 expression is regulated during cell cycle progression [20]. Therefore, it is possible that in addition to its regulation at the expression levels, the remaining binding pocket on PCNA is employed to recruit the ubiquitination machinery to regulate the turnover of the methyltransferase.

Crystal structure of PCNA in complex with ATXR6 PIP motif

To understand the molecular interactions mediating the ATXR6:PCNA complex, we solved the crystal structure of *At*PCNA in complex with *Gm*ATXR6 PIP motif at 2.06 Å using molecular replacement (Table 1). The crystal lattice has a *P*1 space group arrangement, and the asymmetric unit contains six polypeptide chains of PCNA and six chains corresponding to the ATXR6 PIP motif. Of the 19 amino acids belonging to the ATXR6 peptide (residues 78–96), we unambiguously modeled 13 residues (78–90) in the electron density map, whereas residues 91 to 96 had no electron density and were omitted from the structure.

The structure of the PCNA trimer shows a multifaceted three-lobed disc with a circular hole at the center (Fig. 2a and b). The monomeric unit has distinct topologies and is connected to other monomers in an N- to C-terminal fashion (Fig. 2a and c). Each monomer houses an arc-shaped region formed by four slanted α-helices, which line the central hole ring of the trimeric unit where DNA interaction is possible. The back of each inner ring arch is supported by a second and opposite-facing arch formed by a twisted nine-stranded antiparallel blade composed of β2–4, β6, β10, β14, and β16–18, which runs the length of the monomer. Two additional antiparallel blades encompass the arches on the sides of the molecule: a 5-stranded β sheet (β1, β5, β7–9) located at the N-terminal side of the monomer, and at the opposite side, near the

Table 1. Data collection and refinement statistics for the ATXR6 PIP/PCNA complex.

PDB accession number	6O09
Data collection	
Space group	*P*1
Cell dimensions	
a, *b*, *c* (Å)	72.9, 90.5, 90.5
α, *β*, *γ* (°)	60.0, 73.4, 73.5
Resolution	29.65–2.06 (2.13–2.06)[a]
R_{meas}	0.06 (0.36)
$I/\sigma I$	9.1 (2.1)
Completeness (%)	94.4 (91.1)
Redundancy	1.9 (1.8)
CC1/2	0.99 (0.59)
Refinement	
Resolution (Å)	29.65–2.06
No. reflections	219,871
R_{work}/R_{free}	0.1970/0.2329
No. atoms	
PCNA	11,252
$ATXR6^{PIP}$	659
Water	406
B-factors (Å^2)	
Protein	46.7
Ligands	52.8
Water	49.2
R.m.s. deviations	
Bond lengths (Å)	0.007
Bond angles (°)	0.919
Molprobity scores	1.40
Ramachandran favored (%)	2.2
Ramachandran allowed (%)	97.5

[a] Highest-resolution shell is shown in parentheses.

C-terminus, a four-stranded β-sheet (β11–13, β15). In the trimeric unit, at the junction of the monomers, the N-terminal β-sheet of one monomer joins the C-terminal β-sheet of the neighboring monomer to form a larger and continuous antiparallel nine-stranded blade (Fig. 2a) with a similar twist as the central blade (Fig. 2c). These interactions are held in place by backbone hydrogen bonds between β8 (N-terminal sheet) residues Glu115, Asp113 and Ile111, and β13 (C-terminal sheet) residues Thr177, Asn179, and Val181 (Fig. 2a). The central (monomers) and the junctional nine-stranded blades form the outer ring of the PCNA trimer and shield the inner ring composed of 12 α-helices. The outer ring is also made distinct by protrusion of the N/C-terminal loops and an inter-blade connector loop that extends the length of the monomer in front of the central blade connecting β9 and β10 (Fig. 2a).

The crystal structure reveals that one molecule of the ATXR6 PIP motif occupies a binding site located on each PCNA monomer (Fig. 2a). On PCNA, the binding site spans the space that is surrounded by and in close proximity to the long inter-blade loop, the C-terminal loop, and the loops connecting β3–β4 and β16–β17 of the central blade (Fig. 2a). The PCNA trimer disk can be distinguished by two faces: a top surface on which the PIP-motif binding sites appear (Fig. 2a and b) and a reverse side opposite to the PIP binding motif. The peptide predominantly adopts an extended conformation, with a 1-turn 3_{10} helix spanning residues I85, D86, and F87 (single-letter residues denote the peptide) facilitated by intra-molecular interactions in which the amide groups of both F87/88 engage in a hydrogen bond with the carbonyl group of I85, and hydrogen bond with K83 and D85 carbonyl and amine groups, respectively (Fig. 2c and d).

Within the PIP binding pocket of PCNA, two pockets and a shallow groove appear as key interaction sites. The large PCNA pocket is formed by several residues located in the β3–β4 connecting loop and the inter-blade loop (Fig. 2a). The large pocket and its adjacent shallow groove, which lies atop the β16–β17 loop (Fig. 2a), are lined with multiple hydrophobic residues including Leu126 and Ile128 (Fig. 2c and d). In the PCNA:ATXR6 PIP complex, ATXR6 I84 and F87 are buried in the large pocket and F88's phenyl ring lays flat in the shallow groove. Comparative analysis of PIP-bound PCNA structures of ATXR6, FEN-1 [28], DNA Polymerase δ p66 [29], and spartan (SPRTN/DVC-1) [30] (Fig. 3a and b) reveals a shared mode of binding in which the shallow groove is occupied by a bulky hydrophobic residue, while the large pocket accommodates one bulky and one non-bulky hydrophobic residues. Moreover, the short 3_{10} helix is common to other PIP motifs (not shown) and appears to orient the hydrophobic residues of the motif in such a way that they contact the hydrophobic patch of PCNA (Fig. 3a and b).

The smaller binding pocket is positioned between the β3–β4 connecting loop and the C-terminal loop. In the small aperture of this pocket, ATXR6 Q81 makes (Fig. 2c and d) key hydrogen bonds between its side chain's amide group and the carbonyl of Ala-252 (Fig. 2d). The binding mode and the residue, a glutamine, interacting with PCNA small binding pocket are conserved, as similar interactions are observed in the PIP motif of FEN-1 [28], DNA polymerase δ p66 [29], and SPRTN/DVC-1 [30] (Fig. 3a and b). Complementary to this conserved interaction, PCNA C-terminal loop engages three additional backbone to backbone hydrogen bonds with the N-terminal residues of the PIP motif. These interactions hold the two un-ordered loops together in a parallel β-sheet-like manner and involve one hydrogen bond between Pro253 carbonyl group and the amide of T82 while V80 and Ile255 main chains share two hydrogen bonds. The PIP motif is further stabilized by hydrogen bonds between K83 ε-amine and the hydroxyl group of Ser43, located in the β3–β4 connecting loop, as well as R89 carbonyl group of the amide of Gly127. Consistent with the large set of interactions, isothermal calorimetry (ITC) shows that ATXR6 PIP motif binds to PCNA (Fig. 4) with a dissociation constant

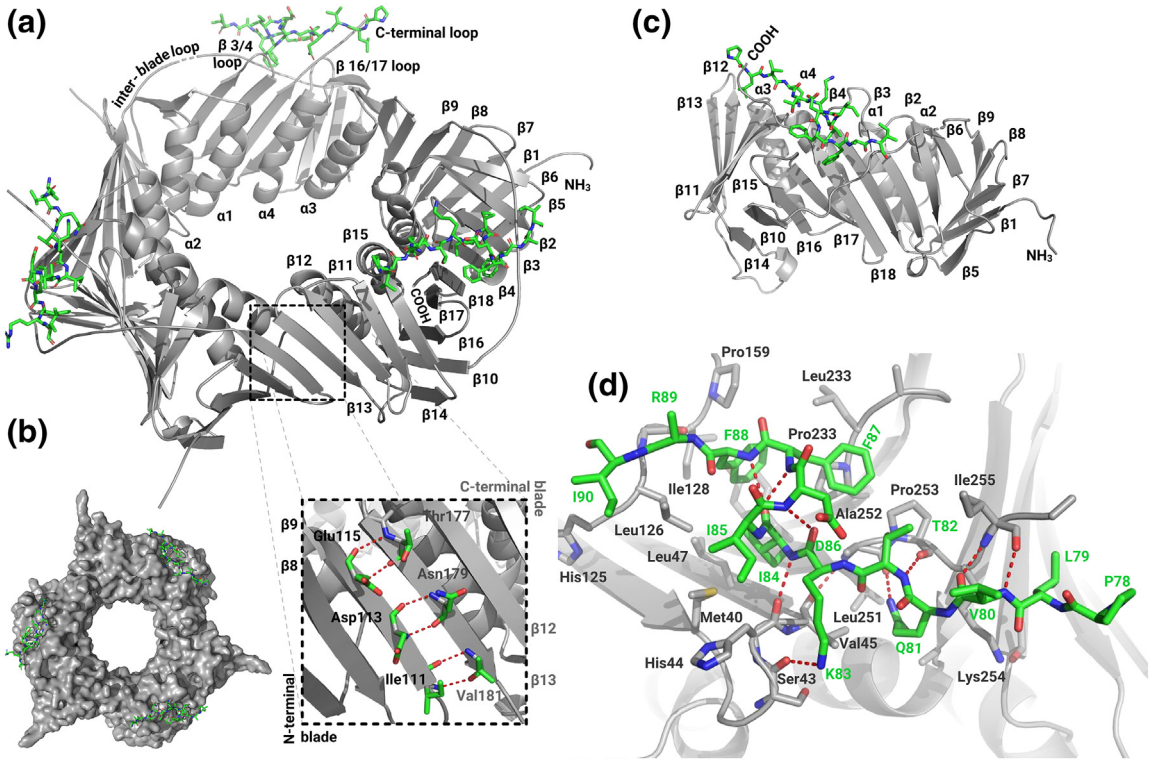

Fig. 2. Crystal structure of ATXR6 PIP motif in complex with PCNA. (a) Cartoon representation of a PCNA trimer bound to three ATXR6 PIP motifs. Labeled β-sheets are indicated on a single PCNA monomer, while loops and α-helices are labeled on a neighboring monomer. ATXR6 PIP motif is highlighted as stick. Carbon, oxygen, and nitrogen atoms are colored in green, red, and blue respectively. A close-up view of the junction between two PCNA monomers is indicated as a panel showing the N-terminal blade of one monomer and the C-terminal blade of the neighboring monomer. Hydrogen bonds are rendered as red dash lines. (b) Surface representation of the structure shown in panel A. (c) Cartoon representation of a single PCNA monomer. (d) Zoomed view of *At*PCNA PIP binding pocket (gray) and ATXR6 PIP motif (green) highlighting the molecular interactions.

of ~1.1 μM, binding affinities that are comparable to the PIP motif of PARG [31] and Pol η [32] within 2- to 3-fold differences.

PCNA inhibits nucleosome methylation by ATXR6

Mutation of *At*ATXR5 PIP motif disrupts H3K27 methylation in plants [12] and the enzyme preferentially mono-methylates histone H3 when incorporated in the NCP over its free form [14]. To test the interplay between the binding of ATXR6 to PCNA and NCP mono-methylation by the enzyme, we performed histone lysine methyltransferase assays either in the absence or in the presence of the sliding clamp. As shown in Fig. 5a, in the absence of PCNA, ATXR6 methylates the NCP. However, increasing concentration of PCNA results in a progressive loss of NCP methylation by ATXR6. Accordingly, the inhibitory effect of PCNA on ATXR6 I103R enzymatic activity is lower when compared to wild-type (Fig. 5b), suggesting that the interaction of PCNA with ATXR6 negatively regulates histone H3 methylation. To test whether PCNA prevents the binding of the cofactor or impairs the formation of the methyltransfer pore, we performed methyltransferase assays using a peptide corresponding to the ATXR6 methylation site (histone H3.1 18–35). As shown in Fig. 5c, increasing concentration of PCNA does not prevent the methylation of the peptide, suggesting that the binding of PCNA to ATXR6 does not directly affect its methyltransferase activity but rather prevents its association to the nucleosome. To further demonstrate this idea, we performed electromobility shift assays (EMSAs) with ATXR6 and nucleosome either in presence or absence of PCNA. Our results show that the addition of PCNA prevents the association of ATXR6 to the nucleosome as illustrated by the similarity in the migration profile between the sample devoid of the methyltransferase and the excess of the sliding clamp (Fig. 5d).

Previous studies revealed that mutation of ATXR5/6 PIP motif leads to a complete loss of methylation in plant, and this effect was initially attributed to the inability of the mutant to associate with PCNA and methylate histone H3.1 during the passage of the replication machinery. However, our studies show that PCNA blocks the methyltransferase activity of ATXR5/6 on the NCP. These observations are

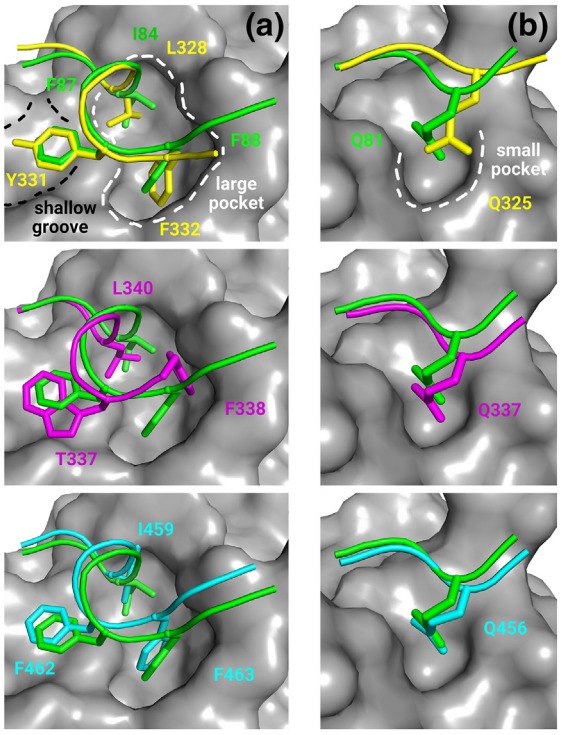

Fig. 3. Comparative analysis of PIP:PCNA complexes. Close-up view of (a) the large binding pocket and the shallow groove as well as the (b) small binding pocket of PCNA. Panels compare the PIP motifs of ATXR6 (green), FEN-1 (5DAI; magenta), DNA polymerase δ p66 (1U76; cyan), and SPRTN/DVC1 (5IY4; yellow). Images were produced using PyMOL by retrieving available structures fetching PDB IDs and aligning associated PCNA molecules with the PCNA structure from this work.

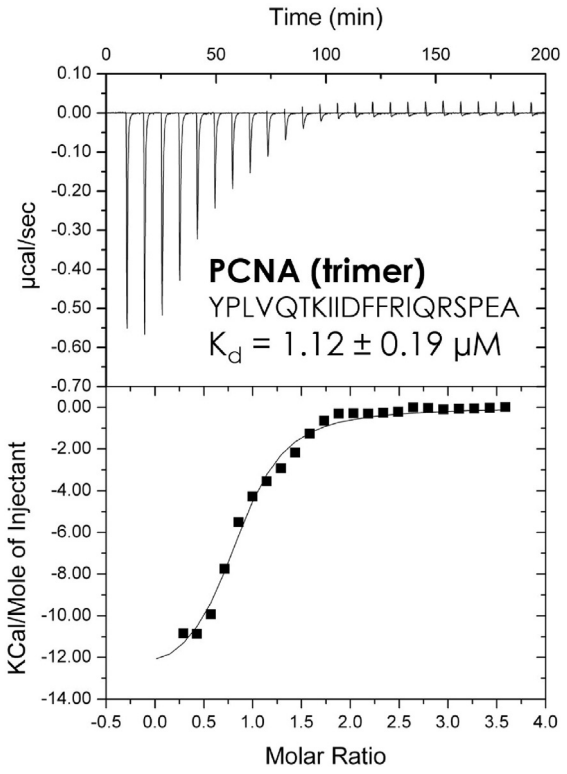

Fig. 4. ATXR6 PIP motif binds with high affinity to AtPCNA. Isothermal titration calorimetry curve of ATXR6 PIP titrated into PCNA. The upper and lower panels show the heat of binding for peptide binding and the integrated data, respectively. The calculated *N* value is ~0.9. Calculation was performed assuming that one ATXR6 PIP motif binds to one protomer of PCNA.

reminiscent to the inhibition of the H4K20 methyltransferase SET8 by the sliding clamp [33] and may point to a model wherein PIP containing histone methyltransferase must disengage from PCNA to re-establish epigenetic marks on histones following replication. In such model, PCNA would serve as a carrier that ensures a local concentration of these enzymes at the replication fork. Alternatively, as proposed for SET8 [33], PCNA may outcompete histone methylation at stalled replication forks as a mean to clear the methyltransferase from the locus via the ubiquitin pathway.

Mutations in the PIP-motif of ATXR5/6 disrupt the genomic integrity and H3K27 distribution in plants [12]. In this work, we demonstrate that this conserved motif is essential for ATXR6 interaction with PCNA. Our data also provide a map of the molecular interactions between the motif and PCNA as well as show that PCNA-bound ATXR6 is unable to methylate histone H3.1 K27 in nucleosomes highlighting a potential shared binding region on ATXR5/6 for PCNA and the nucleosome.

Materials and Methods

ATXR6 expression and purification

A codon-optimized construct corresponding to *Morus notabilis* (*Mn*) ATXR6 was cloned into pGST-4 T-1, and the plasmid was transformed in *Escherichia coli* BL21 DE3 Rosetta cells. The following day, several colonies were transferred into 1 L of Luria–Bertani supplemented with 100 µM $ZnCl_2$ and incubated at 37 °C. Once the OD^{600} reached 0.7, protein expression was induced using 0.2 mM IPTG and incubated at 18 °C for 16 h. Following centrifugation, cells were collected in phosphate-buffered saline supplemented with 5 mM βME and cells were lysed by sonication. Following centrifugation of the lysate at 31,000*g* and filtration of the supernatant, the GST–ATXR6 fusion protein was applied onto glutathione Sepharose (Pierce). Following extensive washing steps, the protein-bound resin was TEV cleaved for 16 h at 4 °C in 20 mM Tris (pH 8.0), 500 mM NaCl, and 5 mM βME and collected as flow-through. *Mn*ATXR6 was concentrated and further

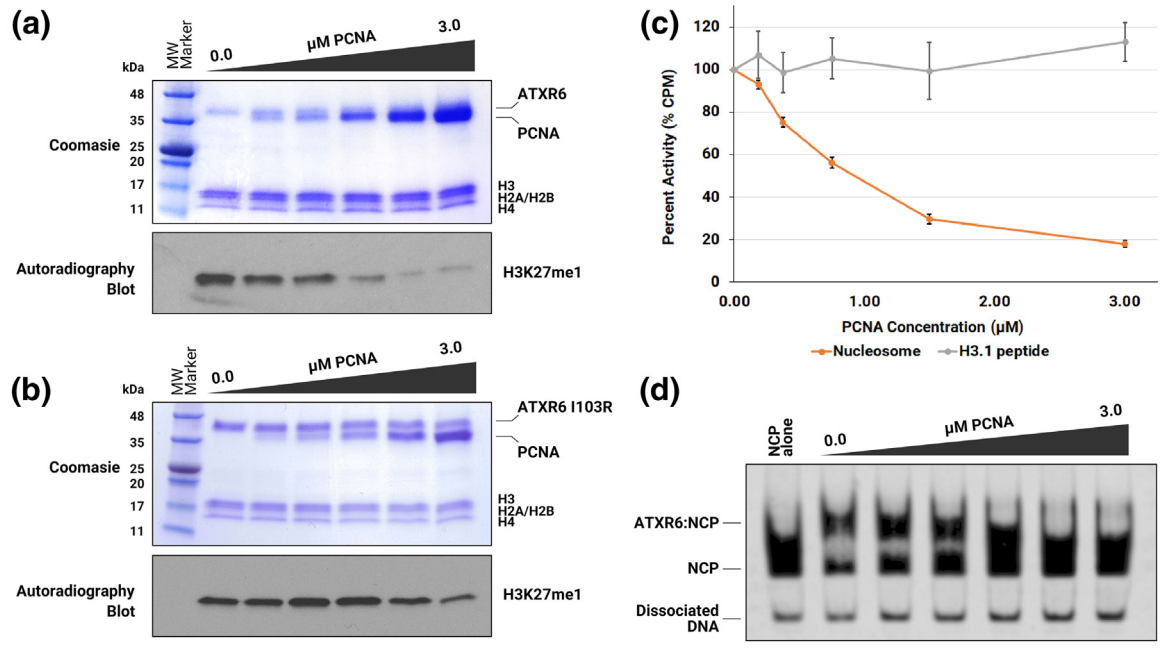

Fig. 5. PCNA inhibits ATXR6 methylation on NCP but not H3.1 peptide. Methyltransferase assays were performed in the absence (0.0 μM) or with increasing concentrations of PCNA (≤3.0 μM) with either wild-type (a) or I103R (b) ATXR6. The top and bottom panels show Coomassie-stained SDS-PAGE gels of each sample and detection of NCP methylation by autoradiography, respectively. (c) Quantitative analysis of nucleosome (orange) or H3.1 18–25 peptide (gray) methylation by scintillation counting either in the absence or in the presence of PCNA. Activity is represented as a percentage of the reactions performed in the absence of PCNA. Error bars indicate the standard deviation of each reaction, which were performed at least three times in triplicate. (d) EMSAs comparing the migration profiles of ATXR6-bound NCP in the absence or presence of an increasing concentration of PCNA.

purified by size exclusion chromatography using a Superdex™ 75 pre-equilibrated in gel filtration buffer [20 mM Tris (pH 8.0), 200 mM NaCl, 5 mM βME]. The protein elutes as a monomer at an apparent molecular weight of 40.1 kDa.

PCNA expression and purification

A codon-optimized construct for bacterial expression corresponding to *Arabidopsis thaliana* PCNA was cloned into pET29(+)a. PCNA was overexpressed for *Mn*ATXR6, and bacterial cell pellets were resuspended and lysed in 50 mM sodium phosphate (pH 7.0), 500 mM NaCl, and 5 mM βME by sonication. Following centrifugation of the lysate at 31,000*g* and filtration, the supernatant was applied on cobalt-agarose (TaKaRa) resin pre-equilibrated in lysis buffer. The beads were washed with 10 column volume of lysis buffer and eluted with the same buffer supplemented with 500 mM imidazole. The eluted protein was concentrated and applied onto a Superdex™ 200 equilibrated with gel filtration buffer. Consistent with its ability to form a trimer, the elution profile shows that PCNA elutes at an apparent molecular weight of ~90 kDa.

Crystallization

A synthetic peptide corresponding to the PIP motif (residues 78–96) of *Glycine max* (*Gm*) ATXR6 was ordered from GeneScript with an extra tyrosine located at the N-terminus to facilitate quantification. The lyophilized PIP peptide was initially suspended in water and subsequently introduced to PCNA in a 2:1 molar ratio in gel filtration buffer. The complex was incubated for 2 h at 4 °C. Crystals were grown in 0.2 M sodium malonate and 20% PEG 3350. Harvested crystals were cryoprotected using Fromblin®, and a full data set was collected using a Rigaku MicroMax-007HF. Images were collected using an R-AXIS IV^{++} detector (Rigaku), and the data set was processed and scaled using Structure Studio (Rigaku). The structure was solved by molecular replacement using Phenix [34] and a search model corresponding to *A. thaliana* PCNA (*At*PCNA; 2ZVV—PDB code) [35]. Six PCNA molecules were modeled in the asymmetric unit. The model was build, refined, and validated using *Coot* [36], Phenix, and Molprobity [37], respectively. Figures of the PCNA/PIP complex were generated using PyMOL Molecular Graphics System (Schrödinger, LLC).

ITC

ITC experiments were performed using a VP-ITC calorimeter (MicroCal) by injecting the peptide (0.22 mM) into a solution of PCNA (10 μM) in gel filtration buffer. The experiment was performed at 20 °C, and the titration data were analyzed using Origin software (OriginLab Corp.). The *Gm*ATXR6 PIP peptide binds to *At*PCNA with a binding stoichiometry (*N* values) of ~0.9 molecule of peptide per monomer of PCNA.

Gel filtration and analytical ultracentrifugation

ATXR6 (WT/mutant) was co-incubated at a 4:1 molar ratio with a PCNA (WT/mutant) trimer in gel filtration buffer. Protein mixtures were applied to a Superdex™ 200 pre-equilibrated with gel filtration buffer. Following size exclusion chromatography, the main peak was concentrated and sedimentation velocity measurements were performed at 20 °C using a Beckman Coulter Optima XL-I analytical ultracentrifuge. Samples were housed in a centrifuge cell equipped with double-sector charcoal-Epon centerpiece. Sedimentation was carried out at 30,000 rpm in an An60-Ti rotor, during which 200 concentration distributions were determined with Abs^{280} optics 180-s intervals. The sedimentation coefficient distribution was determined using the program SEDFIT [38].

Methyltransferase assays

Methyltransferase assays were performed in 25 μL reaction volumes as previously documented [39]. For each assay, ATXR6 (1 μg) was incubated with either NCPs (~0.3 μM) or an H3.1 peptide corresponding to residues 18–36 (20 μM), and tritium-labeled *S*-adenosyl-methionine [^{3}H-SAM] (2 μCi) in a methyltransferase assay buffer composed of 50 mM Tris (pH 8.0), 20 mM KCl, 10 mM $MgCl_2$, 10 mM βME, and 10% glycerol. Methyltransferase assays were performed in the absence or increasing concentration of PCNA (0.0 to 3.0 μM) and incubated at 30 °C for 1 h for NCPs or 20 h for reactions performed with peptides. Reactions were stopped by adding Laemmli buffer and boiling. Quantitative analysis of the methyltransferase assays was performed by spotting the reactions on P81 cellulose filter paper (Reaction Biology Corp.). After drying, filters were washed four times in a 50-mM sodium bicarbonate solution and dried again. Filter papers were sectioned and soaked in 5 mL of ScintiSafe™ Econo1 (Fisher) scintillation liquid prior analysis using a Tri-Carb2910TR (PerkinElmer).

EMSAs

EMSAs were performed as previously described [14]. Briefly, increasing concentration of PCNA (0.0 to 3.0 μM) was added to a binding reaction composed of 1 μg ATXR6, 10 μM Cy5-labeled NCP harboring a K27M mutation, 1 mM AdoHcy, 1% bovine serum albumin, 0.1% Triton-X100, 5 ng/μl poly deoxyinosinic–deoxycytidylic [dI–dC], 50 mM Tris (pH 8.0), 20 mM KCl, 10 mM $MgCl_2$, 10 mM βME, and 10% glycerol. The samples were applied to a 6% native poly-acrylamide gel (60:1).

Accession numbers

Crystallographic data for the ATXR6 PIP/PCNA complex were deposited with the PDB accession number 6O09.

Acknowledgments

This work was supported by a Natural Sciences and Engineering Research Council discovery grant awarded to J.-F.C (RGPIN-2016-04977). We would like to thank Dr. Sabina Sarvan for her technical assistance.

Appendix A. Supplementary data

Supplementary data to this article can be found online at https://doi.org/10.1016/j.jmb.2019.02.020.

Received 11 December 2018;
Received in revised form 15 February 2019;
Accepted 15 February 2019
Available online 28 February 2019

Keywords
Nucleosome;
Proliferating cell nuclear antigen;
Histone;
Methylation;
SET

Abbreviations used:
SET, Su[var], E[z],Trithorax domain; H3K27, histone H3 lysine-27; ATXR, *Arabidopsis* trithorax-related protein; NCP, nucleosome core particle; PCNA, proliferating cell nuclear antigen; PIP, PCNA-interacting peptide; FEN-1, flap endonuclease 1; ITC, isothermal calorimetry; EMSA, electromobility shift assay.

References

[1] E.L. Greer, Y. Shi, Histone methylation: a dynamic mark in health, disease and inheritance, Nat. Rev. Genet. 13 (2012) 343.

[2] K. Hyun, J. Jeon, K. Park, J. Kim, Writing, erasing and reading histone lysine methylations, Exp. Mol. Med. 49 (2017) e324.
[3] S. Lanouette, V. Mongeon, D. Figeys, J.F. Couture, The functional diversity of protein lysine methylation, Mol. Syst. Biol. 10 (2014) 724.
[4] N. Saksouk, E. Simboeck, J. Déjardin, Constitutive heterochromatin formation and transcription in mammals, Epigenetics Chromatin 8 (2015) 3.
[5] J. Müller, C.M. Hart, N.J. Francis, M.L. Vargas, A. Sengupta, B. Wild, et al., Histone methyltransferase activity of a *Drosophila* polycomb group repressor complex, Cell. 111 (2002) 197–208.
[6] K. Plath, J. Fang, S.K. Mlynarczyk-Evans, R. Cao, K.A. Worringer, H. Wang, et al., Role of histone H3 Lysine 27 methylation in X inactivation, 300 (2003) 131–135.
[7] Y. Yu, P. Deng, B. Yu, J.M. Szymanski, T. Aghaloo, C. Hong, et al., Inhibition of EZH2 promotes human embryonic stem cell differentiation into mesoderm by reducing H3K27me3, Stem Cell Rep. 9 (2017) 752–761.
[8] L.O. Baumbusch, T. Thorstensen, V. Krauss, A. Fischer, K. Naumann, R. Assalkhou, et al., The *Arabidopsis thaliana* genome contains at least 29 active genes encoding SET domain proteins that can be assigned to four evolutionarily conserved classes, Nucleic Acids Res. 29 (2001) 4319–4333.
[9] Y. Jacob, S. Feng, C.A. LeBlanc, Y.V. Bernatavichute, H. Stroud, S. Cokus, et al., ATXR5 and ATXR6 are H3K27 monomethyltransferases required for chromatin structure and gene silencing, Nat. Struct. Mol. Biol. 16 (2009) 763.
[10] F. Pontvianne, T. Blevins, C. Chandrasekhara, W. Feng, H. Stroud, S.E. Jacobsen, et al., Histone methyltransferases regulating rRNA gene dose and dosage control in *Arabidopsis*, Genes Dev. 26 (2012) 945–957.
[11] D. Latrasse, T. Jégu, P.-H. Meng, C. Mazubert, E. Hudik, M. Delarue, et al., Dual function of MIPS1 as a metabolic enzyme and transcriptional regulator, Nucleic Acids Res. 41 (2013) 2907–2917.
[12] Y. Jacob, H. Stroud, C. LeBlanc, S. Feng, L. Zhuo, E. Caro, et al., Regulation of heterochromatic DNA replication by histone H3 lysine 27 methyltransferases, Nature. 466 (2010) 987.
[13] Y. Jacob, E. Bergamin, M.T.A. Donoghue, V. Mongeon, C. LeBlanc, P. Voigt, et al., Selective methylation of histone H3 variant H3.1 regulates heterochromatin replication, Science. 343 (2014) 1249–1253.
[14] E. Bergamin, S. Sarvan, J. Malette, M.S. Eram, S. Yeung, V. Mongeon, et al., Molecular basis for the methylation specificity of ATXR5 for histone H3, Nucleic Acids Res. 45 (2017) 6375–6387.
[15] S. Hasan, P.O. Hassa, R. Imhof, M.O. Hottiger, Transcription coactivator p300 binds PCNA and may have a role in DNA repair synthesis, Nature. 410 (2001) 387.
[16] L.S.-H. Chuang, H.-I. Ian, T.-W. Koh, H.-H. Ng, G. Xu, B.F.L. Li, Human DNA–(cytosine-5) methyltransferase–PCNA complex as a target for $p21^{WAF1}$, 277 (1997) 1996–2000.
[17] T.R. Ben-Shahar, A.G. Castillo, M.J. Osborne, K.L.B. Borden, J. Kornblatt, A. Verreault, Two fundamentally distinct PCNA interaction peptides contribute to chromatin assembly factor 1 function, Mol. Cell. Biol. 29 (2009) 6353–6365.
[18] R.A. Poot, L. Bozhenok, D.L.C. van den Berg, S. Steffensen, F. Ferreira, M. Grimaldi, et al., The Williams syndrome transcription factor interacts with PCNA to target chromatin remodelling by ISWI to replication foci, Nat. Cell Biol. 6 (2004) 1236.
[19] A P, X. Xu, C. Wang, J. Yang, S. Wang, J. Dai, et al., EZH2 promotes DNA replication by stabilizing interaction of POLδ and PCNA via methylation-mediated PCNA trimerization, Epigenetics Chromatin 11 (2018) 44.
[20] C. Raynaud, R. Sozzani, N. Glab, S. Domenichini, C. Perennes, R. Cella, et al., Two cell-cycle regulated SET-domain proteins interact with proliferating cell nuclear antigen (PCNA) in *Arabidopsis*, Plant J. 47 (2006) 395–407.
[21] C.M. Kondratick, J.M. Litman, K.V. Shaffer, M.T. Washington, L.M. Dieckman, Crystal structures of PCNA mutant proteins defective in gene silencing suggest a novel interaction site on the front face of the PCNA ring, PLoS One (2018) e0193333.
[22] C. Indiani, P. Mclnerney, R. Georgescu, M.F. Goodman, M. O'Donnell, A sliding-clamp toolbelt binds high- and low-fidelity DNA polymerases simultaneously, Mol. Cell 19 (2005) 805–815.
[23] D. Dovrat, J.L. Stodola, P.M.J. Burgers, A. Aharoni, Sequential switching of binding partners on PCNA during in vitro Okazaki fragment maturation, Proc. Natl. Acad. Sci. U. S. A. 111 (2014) 14118–14123.
[24] D. Bubeck, M.A.M. Reijns, S.C. Graham, K.R. Astell, E.Y. Jones, A.P. Jackson, PCNA directs type 2 RNase H activity on DNA replication and repair substrates, Nucleic Acids Res. 39 (2011) 3652–3666.
[25] P.A. Hall, J.M. Kearsey, P.J. Coates, D.G. Norman, E. Warbrick, L.S.J.O. Cox, Characterisation of the interaction between PCNA and Gadd45, 10 (1995) 2427–2433.
[26] S. Jørgensen, M. Eskildsen, K. Fugger, L. Hansen, M.S. Yoo Larsen, A.N. Kousholt, et al., SET8 is degraded via PCNA-coupled CRL4(CDT2) ubiquitylation in S phase and after UV irradiation, 192 (2011) 43–54.
[27] T. Abbas, E. Shibata, J. Park, S. Jha, N. Karnani, A. Dutta, $CRL4^{Cdt2}$ regulates cell proliferation and histone gene expression by targeting PR-Set7/Set8 for degradation, Mol. Cell 40 (2010) 9–21.
[28] A.S. Altieri, J.E. Ladner, Z. Li, H. Robinson, Z.F. Sallman, J.P. Marino, et al., A small protein inhibits proliferating cell nuclear antigen by breaking the DNA clamp, Nucleic Acids Res. 44 (2016) 6232–6241.
[29] J.B. Bruning, Y. Shamoo, Structural and thermodynamic analysis of human PCNA with peptides derived from DNA polymerase-δ p66 subunit and flap endonuclease-1, Structure. 12 (2004) 2209–2219.
[30] Y. Wang, M. Xu, T. Jiang, Crystal structure of human PCNA in complex with the PIP box of DVC1, Biochem. Biophys. Res. Commun. 474 (2016) 264–270.
[31] T. Kaufmann, I. Grishkovskaya, A.A. Polyansky, S. Kostrhon, E. Kukolj, K.M. Olek, et al., A novel non-canonical PIP-box mediates PARG interaction with PCNA, Nucleic Acids Res. 45 (2017) 9741–9759.
[32] A. Hishiki, H. Hashimoto, T. Hanafusa, K. Kamei, E. Ohashi, T. Shimizu, et al., Structural basis for novel interactions between human translesion synthesis polymerases and proliferating cell nuclear antigen, 284 (2009) 10552–10560.
[33] T.S. Girish, R.K. McGinty, S. Tan, Multivalent interactions by the Set8 histone methyltransferase with its nucleosome substrate, J. Mol. Biol. 428 (2016) 1531–1543.
[34] P.D. Adams, P.V. Afonine, G. Bunkóczi, V.B. Chen, I.W. Davis, N. Echols, et al., PHENIX: a comprehensive Python-based system for macromolecular structure solution, Acta Crystallogr. D Biol. Crystallogr. 66 (2010) 213–221.
[35] W. Strzalka, T. Oyama, K. Tori, K. Morikawa, Crystal structures of the *Arabidopsis thaliana* proliferating cell nuclear antigen 1

and 2 proteins complexed with the human p21 C-terminal segment, Protein Sci 18 (2009) 1072–1080.
[36] P. Emsley, B. Lohkamp, W.G. Scott, K. Cowtan, Features and development of Coot, Acta Crystallogr. D Biol. Crystallogr. 66 (2010) 486–501.
[37] V.B. Chen, W.B. Arendall, J.J. Headd, D.A. Keedy, R.M. Immormino, G.J. Kapral, et al., MolProbity: all-atom structure validation for macromolecular crystallography, Acta Crystallogr. D Biol. Crystallogr. 66 (2010) 12–21.
[38] P. Schuck, Size-distribution analysis of macromolecules by sedimentation velocity ultracentrifugation and Lamm equation modeling, Biophys. J. 78 (2000) 1606–1619.
[39] E. Bergamin, J.F. Couture, Preparation, biochemical analysis, and structure determination of SET domain histone methyltransferases, Methods Enzymol. 573 (2016) 209–240.